Pergamon

Int. J. Heat Mass Transfer. Vol. 39, No. 8, pp. 1763–1767, 1996

0017-9310/96 $15.00+0.00

0017-9310(95)00228-6

Effect of transverse convex curvature on heat transfer from heated cylinders with axisymmetric backward-facing steps

K. C. KIM

Department of Mechanical and Production Engineering, Pusan National University, Pusan, 609-735, Korea

and

Y. LEE†

Department of Mechanical Engineering, University of Ottawa, Ottawa, Canada K1N 6N5

(*Received* 14 *July* 1994 *and in final form* 16 *May* 1955)

1. INTRODUCTION

Reattaching flows are widely used for heat transfer devices, because they can cause large variations of the local heat transfer coefficient as well as a substantial augmentation of the overall heat transfer. Therefore, a study is not only needed for the prediction of the accurate heat transfer rate in an axisymmetric turbulent boundary layer over the wall of a cylinder with an axisymmetric backward-facing step for the engineering design purpose, but also to identify the fundamental aspect of the transverse convex surface curvature on heat transfer in such flows.

Measurements of heat transfer in reattaching flows have been reported on several flow configurations. The two-dimensional flow past a backward-facing step which represents one of the simple geometries for producing flow separation and reattachment of turbulent boundary layer has been studied extensively by Seban [1], Aung and Goldstein [2] and Vogel and Eaton [3]. Recently, Tsou *et al.* [4] carried out experiments to study the starting process of the heat transfer downstream of a backward-facing step. Kim *et al.* [5] measured the turbulent convective heat transfer around a normal obstruction in a two-dimensional (2D) duct under the condition of a constant wall temperature. The reattachment of the separated flow downstream of an abrupt pipe expansion has been studied by Baughn *et al.* [6].

Axisymmetric reattaching flows are also an important problem in thermal engineering. However, there seem to be very few studies made on the convective heat transfer in such flows. Especially, the combined effect of the transverse convex surface curvature has never been systematically studied.

When the radius of a body is on the same order of magnitude as the thickness of the boundary layer, the transverse convex surface curvature (TVCC) effect becomes significant. Kim *et al.* [7] and Lee and Kim [8] investigated experimentally and analytically the TVCC effect on turbulent fluid flow and heat transfer. These studies have shown that while the effect of the transverse surface *concave* on fluid flow is negligible, that of transverse *convex* curvature is significant. The friction coefficient and Stanton number increased with an increase in the transverse convex surface curvature and were always greater than those for the flat plate.

† Author to whom correspondence should be addressed.

In the present study, an experimental study was made on the effect of TVCC on the turbulent convective heat transfer from a heated cylinder with an axisymmetric backward-facing step. The body upstream of the step has a form of an ellipsoid. A typical flow pattern of axisymmetric separation and reattachment is shown in Fig. 1.

The main objective of the present study is, therefore, to identify the effect of TVCC on turbulent heat transfer and to provide new accurate data on the local heat transfer coefficient along the surface of an axisymmetric convex body with flow separation and reattachment.

2. EXPERIMENTAL APPARATUS

2.1. *Visual study*

2.1.1. *The water tunnel.* The visual study was made to determine the values of x_r in a vertical recirculating-flow water tunnel, having a test section of 2800 mm (L) by 1200 mm (H) by 1800 mm (W) made of high optical quality Plexiglas. The tunnel is preceded by two motors (both 20 kW) and one surface flow acceleration motor (10 kW). The power to the motors was supplied through variable-output current frequency which allowed a speed range of water from zero to 2.0 m s^{-1}. The uniformity of the velocity distribution in the test section was within 1.0% deviation, and the level of the free-stream turbulence was about 2.5% in the range of the velocities studied.

2.1.2. *Test cylinders.* The obstructions of the test cylinders were made of Teflon, its contour machined by an NC lathe and the body of the cylinder of hydrodynamically smooth stainless tubing. The overall alignment of the test cylinder to the flow defines the axial symmetry of the boundary layer. To reduce the effect of flow misalignment with respect to the flow, the angle of attack was estimated using a water level to measure the difference in height from the surface of the cylinder at the upstream and downstream ends of the test cylinder. A test cylinder with various ratios of the diameter was situated 1200 mm from the entrance to the water tunnel. No sidewall flow interference was detected within ± 400 mm of the centerline.

2.2. *Quantitative study*

2.2.1. *The wind tunnel.* The wind tunnel used in the study is a low-speed open-circuit Eiffel-type system. It consists of six separate sections: entrance, contraction, test section,

NOMENCLATURE

c_p	specific heat
d	cylinder diameter
D	obstruction diameter, $d+2H$
h	heat transfer coefficient
H	step height
k	thermal conductivity
Nu	Nusselt number
Re	Reynolds number
St	Stanton number
T	temperature
u	axial fluid velocity
x	axial distance.

Greek symbols

ρ	density.

Subscripts

f	film
H	based on step height
max	maximum
r	reattachment point
w	wall
x	local
∞	free stream.

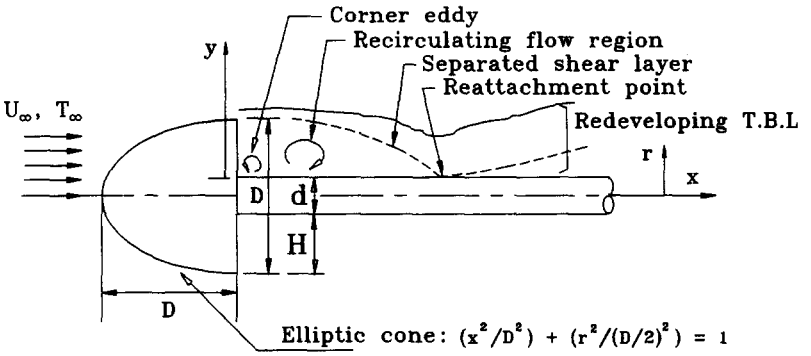

Fig. 1. Flow configuration.

diffuser, flexible coupling and a fan. The 1.53 m × 2.44 m entrance section has four screens made of mesh size 1.4 mm. The first 2.14 m contraction section has a contraction ratio of 4.0. The test section is 3.66 m in length with a rectangular cross-section of 0.91 m × 0.61 m. The rectangular diffuser with an angle of about 6.5° is first converted to a rectangular octagon for a length of 2.29 m and then changed to a 16 sided polygon for a length of 1.07 m. The flexible connection made of about a 300 mm wide rubber band is used to minimize the vibration due to the fan. The Buffalo axial flow fan, type S-54C-9, has a diameter of 1.45 m and the maximum capacity of 25.5 $m^3\ s^{-1}$ at about 89 mm of water and the maximum rpm is 1170. The fan motor has a full load of 26.7 kW and is controlled by an adjustable speed magnetic drive. The blockage effect is negligible on the pressure distribution with test sections used. No blockage correction, therefore, is made for the measured pressure data.

2.2.2. *Test sections.* Three test cylinders (direct electrical resistance heating) and five elliptic cone shape obstructions made of different diameters were used and the essential dimensions are listed in Table 1. The obstructions were made of Teflon bar by contour machining with an NC lathe.

Up to 26 copper–constantan thermocouples (T-type, 30 gauge) were installed using the "split-junction" method [9] along the wall periphery of the test cylinders. Several additional thermocouples were provided on the wall so as to check the symmetry of the temperature distribution. All thermocouples were calibrated *in situ*.

Test sections were positioned in the wind tunnel using two kinds of fixtures; one rigid and fixed for the downstream and the other free, made of piano wire, located at the end of the obstructions. The alignment of the test cylinders with the mean air flow was checked using a survey level and a three-hole yaw tube.

Table 1. Test cylinders and obstructions

Case	d [mm]	L [mm]	D [mm]
1	50.8	1270	102
2	25.4	1016	50.8
			76.2
			102
			127
3	12.7	1016	63.5
			76.2

2.3. *Instrumentation and data reduction*

2.3.1. *Visual study.* Flow visualization was carried out by generating a laser sheet beam in a vertical plane. A thin sheet of light, obtained by spreading a laser beam (Ar-ion, 4 W) by means of a cylindrical lens, illuminates a section of the water flow and scattered radiation is collected and imaged on a photographic film. The 2.3 mm diameter laser beam was focused by collimating lens and expanded in one dimension by a cylindrical lens so as to form a light sheet 1.0 mm thick and 300 mm wide. This sheet of laser is turned 90° by an optical mirror so as to enter a window on the top of the water tunnel vertically. Usual exposure times were between 15 and 30 s for a photographic film with 1600 ASA speed. Neutrally buoyant tracer particles were used to mark the flow. The tracers (polyvinyl chloride) had a specific gravity of 1.02 with diameters ranging between 100 to 200 μm, which was good enough to follow the mean water flow. The particle concentration in the water tunnel was approximately 6 cm^{-3} per ton.

2.3.2. *Quantitative study. Velocity measurement.* The pressure signal from the upstream pitot-static tube was obtained with two MKS Baraton pressure transducers which have a full-scale pressure head of 133.4 Pa (1 torr) and 1.334 kPa (10 torr), respectively, with not more than 0.1% error at full scale. The DC signal is connected to the data acquisition system to be explained below.

Heat flux measurement. The wall of the test cylinder acts as a resistance heating element. Because of the high electric current required, the power to the test cylinder was applied via two transformers in series. The power dissipated in the test cylinder was determined by measuring the electric potential drops and current individually along the test section. For the potential drop measurement, the wires of thermocouples were utilized.

The data acquisition system used in the study consists of a Hewlett-Packard (HP) desk top computer with four other HP instruments: one digital voltmeter, one scanner, one printer/plotter and one real-time clock. The thermocouple EMFs were measured with an HP 3455A digital multimeter to an accuracy of $\pm 5\ \mu V$ ($\pm 0.12°C$).

Data reduction procedure. For the heat transfer study, the power input to the test cylinder was regulated so that the difference between the average surface temperature and free stream air temperature was between 15 and 20°C. At the location on the cylinder wall where the maximum heat transfer rate occurred, the temperature difference was only about 6–7°C. With the uncertainties in the temperature measurements the corresponding uncertainties in the maximum Nusselt numbers due to the temperature measurements were about $\pm 2\%$. A duration of up to 60 min was normally required to reach the steady-state condition. The tests were carried out for free-stream air velocities between 5 and 30 m s^{-1} and the reproducibility of the experimental results was checked by performing a number of test runs at the same condition.

Because of the axial heat conduction due to the different flow regimes, the condition of constant heat flux is no longer applicable, especially for small values of x, even with electrical resistance heating. Therefore, the local heat transfer coefficient was deduced from an equation, which was derived from an energy balance made on the element of the test cylinders [9]. The values of the second derivatives of temperature in the equation were determined from the experimental results of the axial temperature distribution. The maximum error introduced in the final values of the heat transfer coefficients by neglecting the axial heat conduction was, however, less than 1% at the reattachment point. The maximum effect of the radiation was seen to be about 0.4%.

The local Nusselt and Stanton numbers are defined, respectively, as

$$Nu_H = \frac{h_x H}{k_f} \tag{1}$$

and

$$St_x = \frac{h_x}{\rho_f c_p u_\infty} \tag{2}$$

where the local film temperature is defined as $0.5(T_{w,x}+T_\infty)$.

3. RESULTS AND DISCUSSIONS

The measured axial variation of the local Nusselt number is shown in Fig. 2 for the three diameter ratios with the same step height over a range of Reynolds numbers. The symbols in Fig. 2 are the calculated points from the experimental data and have been connected with straight lines by a computer graphics program. Generally, the results display the similar features observed in a 2D case, i.e. a drop in heat transfer at the separation, followed by a sharp rise in the reattachment zone and the peak heat transfer coefficient occurring near

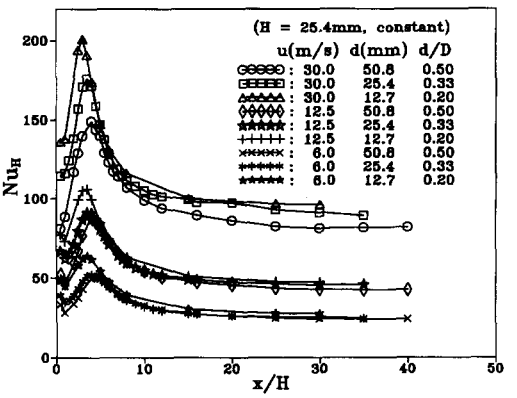

Fig. 2. Local Nusselt number distribution (constant step height, $H = 2.54$ mm).

the mean reattachment point. In the present case, it was observed that the reattachment lengths are shorter than those of the 2D cases and decrease with decreasing cylinder radius. The most striking feature of the present case is that the maximum Nusselt numbers increase with decreasing cylinder radius at the conditions of same step height and flow velocity. It was also observed that the heat transfer in the recirculating flow region increases with an increase in the convex surface curvature [i.e. decreasing $d/D = d/(D+2H)$], but, in the redeveloping region, the Nusselt number decreases more rapidly with an increase in the surface convex curvature. This may be due to the fact that the vertical fluctuations of turbulent eddies quickly attenuated when the thickness of the boundary layer becomes thicker than the local radius of an axisymmetric body.

The variation of the local Nusselt number very near the corner region shows a different nature with respect to the Reynolds number. For the cases of relatively small Reynolds number, a minimum value of Nusselt number occurs at approximately one step height from the step, a feature that strongly suggests the presence of a counter-rotating eddy trapped in the corner. Baughn *et al.* [6] also observed the same phenomenon in their local heat transfer measurements downstream of an abrupt expansion in a circular pipe.

Figure 3 shows the variation in the position of the maximum Nusselt number for various diameter ratios, d/D, at the conditions of the same flow velocity and cylinder diameter. The smaller the value of d/D, the shorter the distance to the maximum heat transfer. For the two largest step heights (i.e. $d/D = 0.333$ and 0.25), the minimum value of Nu_H occurs at about one step height from the step. This also

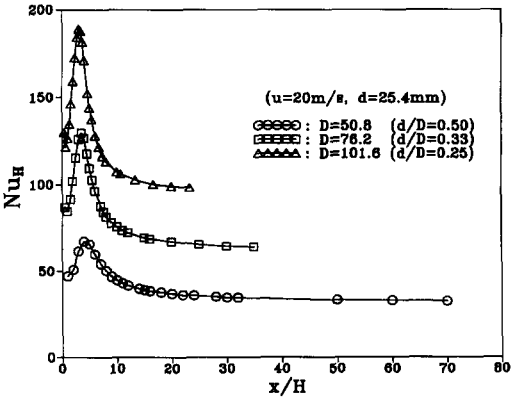

Fig. 3. Local Nusselt number distribution (constant cylinder diameter, $d = 2.54$ mm).

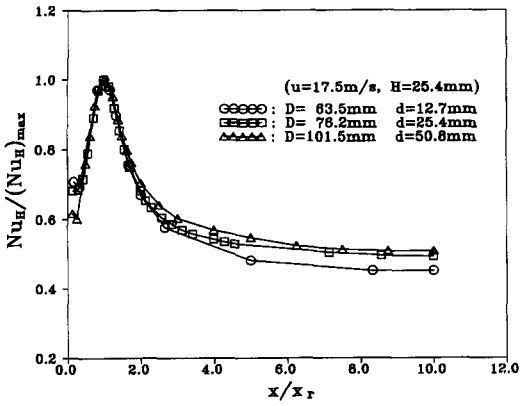

Fig. 4. Normalized Nusselt number (H = constant, 25.4 mm).

implies the presence of a corner eddy trapped due to the larger and more active recirculating flow region.

The normalized Nusselt number by its maximum value vs the normalized axial distance for the case of the same step height and flow velocity are presented in Fig. 4. A similarity nature is observed in the reattachment region ($0.5 < x/x_r < 1.5$). The TVCC effects, however, definitely appear in the corner eddy and the redeveloping boundary layer region. It can be explained that the heat transfer mechanism in the reattachment region may be mainly due to the shear layer impingement process in which the TVCC effect is relatively small. In the redeveloping region, the normalized Nusselt number decreases more rapidly with the decreasing cylinder diameter although the local Nusselt numbers have higher values with the decreasing cylinder radius at the same axial position. This indicates that the TVCC effect promotes the boundary layer relaxation process in the redevelopment region. The increase of the heat transfer in the corner eddy is also related to the TVCC effect, because the velocity gradient near the wall becomes steeper as the cylinder radius becomes smaller [7].

The normalized Nusselt number distributions under the condition of the same cylinder diameter and flow velocity also showed the similarity nature in the overall heat transfer distributions when the maximum Nusselt number and the reattachment length are used as the characteristic parameters, except for the initial redeveloping region. It was seen that the Nusselt Number quickly reduced to the boundary layer value as the TVCC effect becomes significant (i.e. decreasing d/D). For all combinations of the cylinders and obstructions, it was seen that as the Reynolds number is progressively increased, the values of the maximum Nusselt number increase monotonically.

The maximum Nusselt number from the present experiments is plotted in Fig. 5 as a function of Reynolds number based on the step height. The line indicates an exponent of 2/3, which is one of the usual correlations of 2D cases. It can be seen that the effect of the diameter ratio, d/D, on the value of Nu_{max} is rather significant. It seems that the exponent decreases with the decreasing cylinder radius.

The following empirical correlation was deduced from the present study which includes the transverse convex surface curvature effect:

$$(Nu_H)_{max} = [0.113 - 0.091(d/D)]\, Re_H^{2/3}. \quad (3)$$

The standard deviation of equation (3) is about 3.5%.

A comparison with the measurements of Vogel and Eaton [3] for the case of a 2D backward-facing step is given in Fig. 6. In the present experiments, it was seen that the reattachment point is located about 4 step heights downstream of the separation while the reattachment point was about 6.7 step heights in the 2D case. At the same Reynolds number, the maximum Stanton numbers are always greater than those for the 2D backward facing step flow. It is concluded that the effect of the transverse convex surface curvature of the heated cylinders is to increase heat transfer more than that of the 2D reattaching flows. Therefore, the effect must be taken into account when a predictive method is to be applied to fluid flow and heat transfer from an axisymmetric convex body with an obstruction.

4. CONCLUSIONS

(1) The reattachment lengths of the flow over the cylinders with axisymmetric backwards-facing steps are always shorter than those of the 2D and are decreasing with decreasing cylinder radius and increasing Reynolds number.

(2) At the conditions of the same step height and flow velocity, the maximum Stanton numbers increase with decreasing value of the cylinder radius and are always greater than those for 2D backward-facing flow.

(3) The heat transfer in the recirculating flow region increases with an increase in the radius convex curvature, but in the redeveloping region, Stanton number decreases more rapidly with decreasing cylinder radius.

Acknowledgements—This study was carried out under the International Scientific Exchange Award Program between Korean Science and Engineering Foundation (KOSEF) and Natural Science and Engineering Research Council of Canada (NSERC).

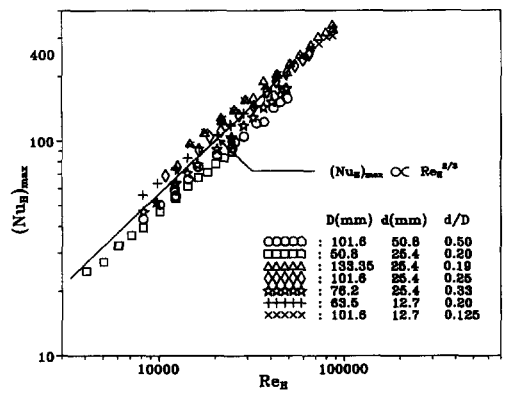

Fig. 5. Reynolds number dependency on the maximum Nusselt number.

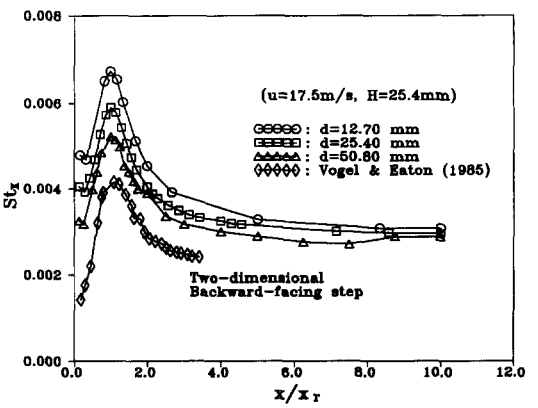

Fig. 6. Comparison with 2D backward-facing step flow.

REFERENCES

1. R. A. Seban, Heat transfer to the turbulent separated flow of air downstream of a step in the surface of a plate, *ASME J. Heat Transfer* **42,** 259–264 (1964).
2. W. Aung and R. J. Goldstein, Heat transfer in turbulent separated flow downstream of a rearward facing step, *Israel J. Technol.* **10,** 35–41 (1971).
3. J. C. Vogel and J. K. Eaton, Combined heat transfer and fluid dynamics measurements downstream of a backward-facing step, *ASME J. Heat Transfer* **107,** 922–929 (1983).
4. F. K. Tsou, S. J. Chen and W. Aung, Starting flow and heat transfer downstream of a backward-facing step, *ASME J. Heat Transfer* **113,** 583–589 (1991).
5. K. C. Kim, M. K. Chung and Y. Kim, Turbulent convective heat transfer around a normal fence in a two-dimensional duct, *Int. Commun. Heat Mass Transfer* **14,** 531–542 (1987).
6. J. W. Baughn, M. A. Hoffman, R. K. Takahashi and B. E. Launder, Local heat transfer downstream of an abrupt expansion in a circular channel with constant wall heat flux, *ASME J. Heat Transfer* **106,** 789–796 (1984).
7. K. C. Kim, Y. Lee and E. Ma, Effect of transverse convex curvature on turbulent flow and heat transfer, *Proceedings of 1st International Symposium Exp. & Comp. Aerothermodynamics of Internal Flows*, Beijing, pp. 202–207 (1990).
8. Y. Lee and K. C. Kim, Analysis on effect of transverse convex curvature on turbulent fluid flow and heat transfer, *Wärme- und Stoffübertragung* **28,** 89–95 (1993).
9. Y. Lee and U. Mital, A two-phase closed thermosyphon, *Int J. Heat Mass Transfer* **15,** 1695–1707 (1972).

Pergamon

Int. J. Heat Mass Transfer. Vol. 39, No. 8, pp. 1767–1769, 1996

0017-9310/96 $15.00+0.00

0017-9310(95)00230-8

Thermal erosion of magnetoplasmadynamic thruster cathode

R. C. MEHTA†
Aerodynamics Division, Vikram Sarabhai Space Centre, Trivandrum 695022, India

and

S. ANDREWS and P. V. RAMACHANDRAN
Department of Mechanical Engineering, College of Engineering, Trivandrum 695016, India

(*Received in final form* 27 *October* 1994)

INTRODUCTION

The magnetoplasmadynamic (MPD) arcjet finds many practical applications in the areas of electric space propulsion, plasma spray and metal cutting torches, etc. In the spacecraft, the MPD arc thrusters operate at large discharge electric current and low mass flow rates in order to obtain high specific impulse and thrust efficiency. For these space applications, a life time of 10^7 cycles ($\sim$100 days) would be demanded for the space MPD thruster [1]. In this condition, the MPD thruster would be exposed to severe thermal environments, thus, resulting in a sharp temperature rise at the cathode root due to the pulsed heat inputs which largely affect electrode erosion and electron emission. It is required for satisfactory and reliable operation of the thruster, that the cathode be operated at a high temperature at the cathode tip to allow the emission of electrons with a moderate electric field, so as to suffer minimum material loss. But severe surface thermal erosion at the cathode tip has been noticed experimentally in transient as well as steady state operating conditions.

Shih *et al.* [2] have not considered the conical shape of the cathode in their analysis of heat conduction problem with radiation and also its effect on the temperature profile. In practice, a 2% thoriated tungsten cathode whose $L/2r$ ratio varies from 1.5 to 3.0 with a semi cone angle of 15–30° (see in Fig. 1) is commonly used in cascade and MPD arc devices. Thermal phenomena on the electrode surface have been analyzed numerically and experimentally by Kuwahara *et al.* [3]. They solved numerically, the unsteady heat conduction equation using finite difference method under periodic heat input condition over a flat plate. The conical shape cathode has been analysed previously using Runge–Kutta method [4] and finite difference scheme [5], without considering the thermal erosion of the cathode material.

The objective of this paper is to present a numerical solution of the heat transfer problem of conical shape cathode. A deforming element technique [6] is applied to take into account ablation of the cathode material. The solution is advanced by fully explicit time-stepping in conjunction with the finite element method.

PROBLEM FORMULATION

Consider a cathode with a varying cross-section area and with constant thermophysical properties. The configuration of a MPD thruster is illustrated in Fig. 1. The energy equation

† Author to whom correspondence should be addressed.